

Bands and bonds of B_{12}

Seongbok Lee, D. M. Bylander, and Leonard Kleinman
 Department of Physics, University of Texas, Austin, Texas 78712
 (Received 26 February 1990)

Using an expansion of ~ 2870 plane waves, we have performed *ab initio* calculations of the energy bands, equilibrium lattice constants and atomic positions, and cohesive energy of B_{12} . We find an indirect gap of 1.427 eV and a direct gap of 1.780 eV. The lattice constants and atomic positions are in good agreement with x-ray data, and charge-density contour plots reveal strong intricosahedral and interplanar intericosahedral bonding but weak intraplanar intericosahedral bonding.

I. INTRODUCTION

This is the second in a planned series of four papers on boron and its carbides, all of which are based on the boron icosahedron of Fig. 1. Of all the polymorphs of elemental boron B_{12} is the simplest.¹ Consider a trigonal lattice obtained from an fcc lattice by stretching it along the [111] axis so as to reduce the angle α between the primitive lattice vectors from 60° to about 58° . On each lattice site place a boron icosahedron, allowing it to distort while maintaining D_{3d} symmetry but losing its five-fold rotation axis. Each top (t) bonds to a bottom (\hat{t}) atom in the plane above and each equatorial atom e (\hat{e}) forms a triangular bond with e (\hat{e}) atoms from two other icosahedra in the same plane. The carbides $B_{12}C_3$, whose calculation we have recently completed, and $B_{13}C_2$, which we are about complete, are very similar to B_{12} . Increase α to about 65.7° and for $B_{12}C_3$ replace one icosahedral t or \hat{t} boron atom with a carbon and place a CBC chain in the fcc octahedral interstitial site so that it lies along the threefold axis. (See Fig. 1 of Ref. 2.) Our

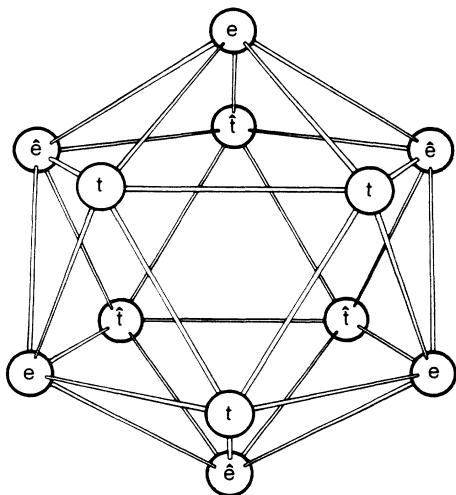


FIG. 1. The boron icosahedron. When distorted in B_{12} it still consists of four equilateral triangles, t , e , \hat{e} , and \hat{t} .

preliminary results indicate the $C_{13}B_2$ differs from $C_{12}B_3$ by replacement of the icosahedral B by a C, although there are others^{3,4} who believe a chain B is replaced by a C. The carbides are thought to have (and our calculations verify) a somewhat larger cohesive energy than elemental boron because boron's interplanar intericosahedral bond is much weaker than the bond between icosahedral and chain atoms. This is mainly due to the longer bond length but also due to the bond direction, which prefers to be radially outward from the icosahedron.¹

α -rhombohedral boron (B_{12}) is unstable when heated above 1200°C and above 1500°C recrystallizes as β -rhombohedral B_{105} which remains stable then at any temperature below the melting point.¹ It is only limitations imposed by the kinetic mechanism for forming B_{105} that allows B_{12} to be stable below 1100°C . Becher⁵ found that heating a mixture of B_{12} and beryllium between 850 and 1000°C results in the boride BeB_{12} and that BeB_{12} reacts with BCl_3 at 375°C to give α -tetragonal boron and BeCl_2 . On the other hand, B_{105} does not react with beryllium even at 1200°C . α -tetragonal boron, B_{50} , will be the subject of the last paper in this series.

Our computational method is that described in the appendices to Ref. 2. Because α is closer to 60° here, our 32-point sample of the Brillouin zone (BZ) is more evenly spaced than for $B_{12}C_3$ but it is somewhat less dense because of the smaller unit cell. We use fewer plane waves here (between 2866 and 2873 at the five points in the irreducible wedge of the BZ) which includes all plane waves with $k^2 < 44.005$ Ry, which is slightly greater⁶ than the cutoff used for $B_{12}C_3$. Otherwise the calculation is identical. Our results are presented in the following section together with a discussion of the nature of the bonding in B_{12} .

II. RESULTS

Table I lists the calculated equilibrium lattice vectors and atomic positions in B_{12} , and Table II compares the magnitude of and angle between the lattice vectors as well as the nearest-neighbor bond lengths with values obtained from x-ray data.⁷ As with $B_{12}C_3$, the lattice constant is less than $\frac{1}{2}\%$ smaller than and the angle is in ex-

TABLE I. Calculated positions of the t and e atoms in B₁₂ relative to the center of an icosahedron and r and s (all in bohr). The \hat{t} and \hat{e} atoms are obtained by inversion of the t and e through the icosahedral center. The primitive lattice translations are $\mathbf{R}_1=(s,0,r)$ and $\mathbf{R}_{2,3}=\frac{1}{2}(-s,\pm\sqrt{3}s,2r)$.

s	$=5.3350$	r	$=7.8753$
t_1	$=(1.8993, 0, 2.5599)$		
t_2	$=(−0.9497, 1.6448, 2.5599)$		
t_3	$=(−0.9497, −1.6448, 2.5599)$		
e_1	$=(−3.1494, 0, 0.5712)$		
e_2	$=(1.5747, −2.7274, 0.5712)$		
e_3	$=(1.5747, 2.7274, 0.5712)$		

cellent agreement with the x-ray value. The agreement for bond lengths is much poorer, but Decker and Kasper⁷ state that it is very difficult to make an assessment of the reliability of the atomic distances from their data, whereas we can see no reason that our atomic separations should be less accurate than our lattice vectors. Although the bond-length orderings are the same, the calculated intraicosahedral bonds have less variation, and the intericosahedral bond lengths are much shorter relative to the experimental ones than the lattice constant difference would imply.

Figure 2 is the energy bands of B₁₂ with the same notation for symmetry points used in Ref. 2. We note that the indirect gap from the top of the valence bands at Z to the bottom of the conduction bands at Γ is 1.427 eV wide, whereas the direct gap at Γ is 1.780 eV wide. Horn⁸ has some optical-absorption data from which he concludes the energy gap is in excess of 2 eV, although from the curve he displays we would place the lowest possible value at 1.8 eV. He also plotted conductivity versus $1/T$ for red and black (presumably due to impurities) B₁₂ and B₁₀₅. The red crystalline B₁₂ conductivity was flat between 290 and 800 K but above 800 K $\log \rho$ had a linear dependence consistent with a 2 eV gap. Note, however, that the temperature dependence of the conductivity is determined by the indirect gap, whereas the optical-absorption edge occurs at the direct gap. Since density functional theory yields gaps that are too small by at least 0.7 eV in the zinc blende and diamond semiconductors and might do so here, there is no inconsistency between theory and experiment.

TABLE II. Calculated lattice constant and angle, and bond lengths of B₁₂ compared with experimental results of Ref. 7 (in bohr).

	Calculated	Experiment
a	9.512	9.556 ± 0.006
α	58.119°	$58.06^\circ \pm 0.05$
tt	3.290	3.269
te	3.391	3.383
$t\hat{e}$	3.371	3.383
$e\hat{e}$	3.350	3.364
$\hat{t}\hat{t}$	3.155	3.231
ee	3.786	3.836

Figure 3 is a plot of contours of constant pseudocharge density in units of millielectrons per cubic bohr (me/a_0^3). The corners of the figure are at the centers of icosahedra, with the shorter sides being the primitive lattice vector \mathbf{R}_1 and the longer sides being $\mathbf{R}_2 + \mathbf{R}_3$, which can also be taken to be a primitive lattice vector. The small 40 me/a_0^3 contours locate the B atoms. Note the two B atoms which lie almost but not exactly on \mathbf{R}_1 . (The preferred angle between bonds emanating from an undistorted icosahedron is that of the fivefold axes which is 63.43° , whereas the \mathbf{R}_i make 58.12° angles with each other.) The interplanar bond between these two atoms has a double peak of $160 me/a_0^3$, whereas the intraicosahedral bond between the second atom and the atom directly below it has a double peak of $120 me/a_0^3$ (actually at $128 me/a_0^3$, as seen in Fig. 4). The most striking difference between this figure and the corresponding one for B₁₂C₃ is the large void at the quasioctahedral interstitial site where the charge density drops below $5 me/a_0^3$. Figure 4 is a contour plot on the three independent (out of 20) icosahedral faces. There is a pseudocharge depletion in

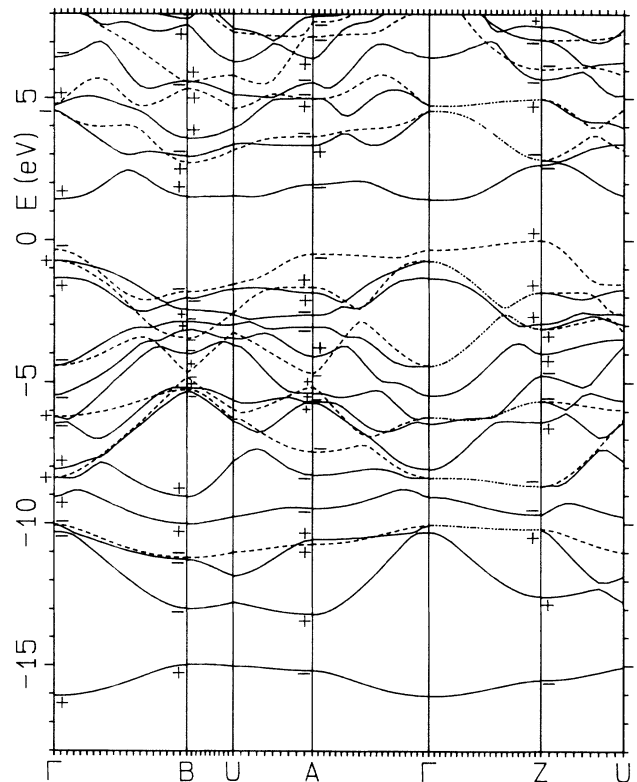


FIG. 2. Energy bands of B₁₂. The solid (dashed) lines represent states which are even (odd) under reflection in a vertical plane. Along the threefold rotation axis from Γ to Z the dotted-dashed lines represent twofold degenerate states. The symmetry under inversion is shown by a + or - at the symmetry points Γ , B, A, and Z. Γ_1^\pm and Z_1^\pm (Γ_2^\pm and Z_2^\pm) states become solid (dashed) lines in any direction, whereas Γ_3^\pm and Z_3^\pm states become either a dotted-dashed line or a pair of lines, one solid and one dashed.

icosahedral bonds can be formed from the B $2s$ and $2p$ orbitals which use up 26 electrons; the six t and \hat{t} borons require an electron each to form their intericosahedral bonds, leaving four electrons, to be shared by the six e and \hat{e} borons to form their Δ bonds. This chemists' picture of bonding should not be taken too seriously for a crystal. If it were rigorously correct, one would expect (at least at Γ where there are no phase factors) that there would be two degenerate (one for each Δ bond in the unit cell) spin degenerate pairs of Δ bonding states, whereas there are four nondegenerate spin-degenerate pairs at Γ which contribute significantly, but not exclusively, to the Δ bonds. Because of inversion symmetry, each contributes identically to the two Δ bonds in the unit cell. We list them here⁹ together with their maximum contour and their charge density at the center of a Δ bond (in me/a_0^3 per spin pair): $\Gamma_1^{+(2)}$ (26, 21), $\Gamma_1^{-(2)}$ (26, 23), $\Gamma_1^{-(3)}$ (20, 19), and $\Gamma_1^{+(4)}$ (11, 10). These add to a peak charge density of

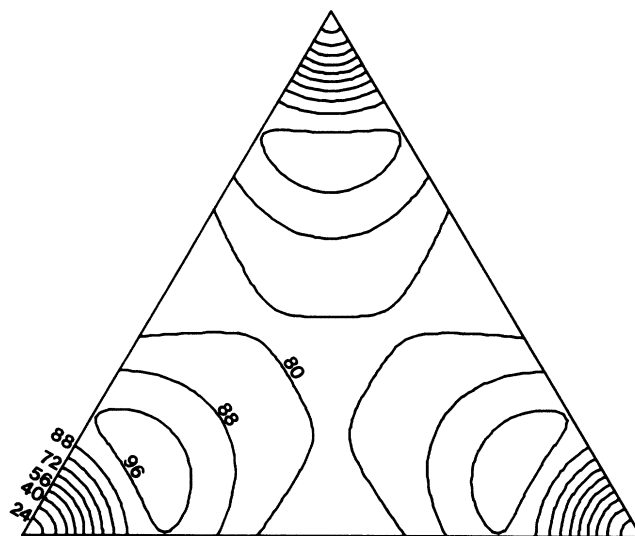


FIG. 6. Contours of constant charge density in steps of $8 me/a_0^3$ in a plane containing three of the weak $e-e$ (or $\hat{e}-\hat{e}$) bonds or, alternatively, a single triangular $e-e-e$ or $\hat{e}-\hat{e}-\hat{e}$ bond.

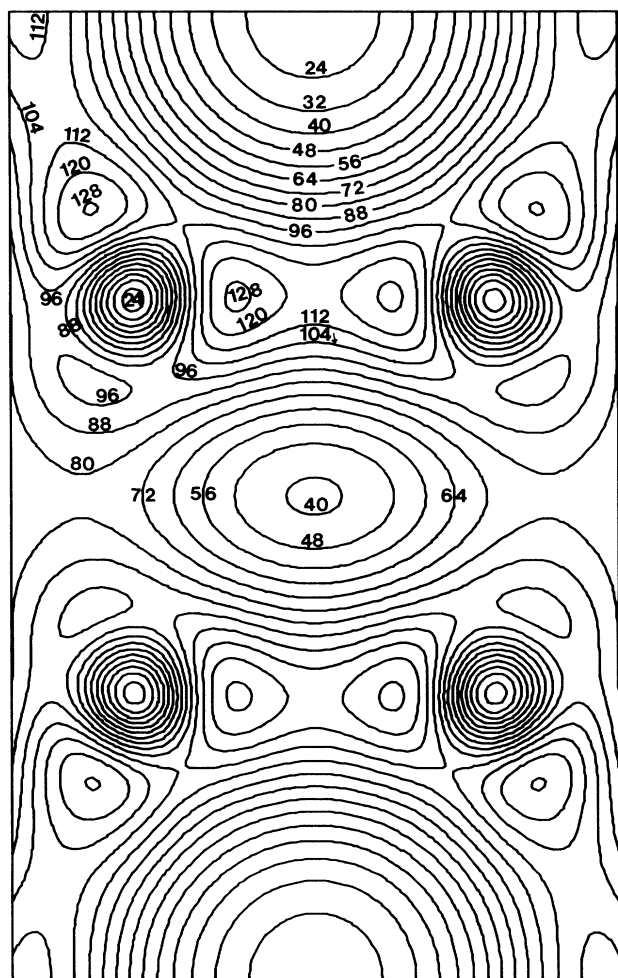


FIG. 5. Contours of constant charge density in steps of $8 me/a_0^3$ in a plane containing $e-\hat{e}$ bonds in two icosahedra and the weak $e-e$ and $\hat{e}-\hat{e}$ intericosahedral bonds.

$83 me/a_0^3$ and a bond center of $73 me/a_0^3$, compared to somewhat above $96 me/a_0^3$ and below $80 me/a_0^3$ for the bond shown in Fig. 6. The difference is due to contributions from the remaining 14 spin pairs. Similarly, the peak charge density of over $160 me/a_0^3$ in the intericosahedral $t-\hat{t}$ bonds would be expected to come from three spin-degenerate pairs. $\Gamma_1^{+(3)}$ contributes $28 me/a_0^3$ and the two degenerate spin pairs of $\Gamma_3^{+(3)}$ contribute $104 me/a_0^3$ but $\Gamma_3^{+(2)}$ also contributes $24 me/a_0^3$ so that the $\Gamma_3^{+(3)}$ can be said to be a pair of $t-\hat{t}$ bonding orbitals, but the third $t-\hat{t}$ intericosahedral bond has contributions from three orbitals which also contribute to intraicosahedral bonding.

The lowest four bands consist not of bonding orbitals, but of cluster orbitals. $\Gamma_1^{+(1)}$ is a cluster s orbital with $7 me/a_0^3$ at the center of the icosahedron, peaking at $11 me/a_0^3$ inside the icosahedron and with $\rho > 8 me/a_0^3$ over most of the center of the ttt and tte faces and $\rho > 9 me/a_0^3$ over the $te\hat{e}$ face. $\Gamma_1^{-(1)}$ is a cluster longitudinal p orbital with $\rho > 32 me/a_0^3$ over the center of the ttt face. $\Gamma_3^{-(1)}$ is the transverse p cluster orbitals. It wants to have large ρ around the belly of the icosahedron but has to avoid the atomic cores. It peaks at $20 me/a_0^3$ inside the icosahedron, at over $13 me/a_0^3$ in a strip outside the e atom core in the tte face and at over $17 me/a_0^3$ in an area between the e and \hat{e} atoms in the $te\hat{e}$ face. The fifth level is $\Gamma_1^{+(2)}$ which contributes to the Δ bond. It also has $\rho > 14 me/a_0^3$ over most of the ttt face and $> 15 me/a_0^3$ over small areas in the face near the atoms. Because only one fact out of ten is a ttt face, this is not a large icosahedral bonding contribution. The remaining levels all contribute to the icosahedral bonding to a greater or lesser extent. For example, the $\Gamma_3^{+(1)}$ states form $e-\hat{e}$ bonds around the icosahedron, each spin pair having a double peak of $17 me/a_0^3$ on each bond, but these states also

contribute charge to the rectangle between $e-\hat{e}$ bonds (Fig. 5). On the other hand, the top of the valence band, $\Gamma_2^{-(1)}$, forms a similar icosahedral bond peaking at $37 me/a_0^3$. Being odd under reflection, this state must vanish between the $e-\hat{e}$ bonds of different icosahedra. The Γ_1^+ state at the bottom of the conduction band is slightly Δ bonding and very strongly bonding in the ttt face of the icosahedron. It grows from near 0 at the t atoms to $30 me/a_0^3$ in the center of the face, unlike most bonding orbitals which peak outside the atomic cores and then fall off very slowly to the face center. The reason this is a conduction-band state is that it is antibonding in the tte face, where it peaks at $15 me/a_0^3$ above the e atom, falls to zero in the middle of the face, and grows to $17 me/a_0^3$ at a double peak along the $t-t$ bond.

Finally, we have calculated the cohesive energies of B_{12} and diamond and list them in Table III along with that previously² calculated for $B_{12}C_3$. Comparing with experiment,¹⁰ $E_{\text{coh}}(B_{12})$ is too large by 1.03 V and $E_{\text{coh}}(C)$ by 1.02 eV. These errors arise from the inadequacy of the local-density approximation for exchange and correlation, especially for the atomic energies, which are subtracted from the crystal energies to obtain the cohesive energies. Even in the crystal the errors tend to be atomistic rather than bonding so that the relative cohesive energies of C and B_{12} are in excellent agreement with experiment. As expected, the B_{12} cohesive energy is considerably smaller than that of $B_{12}C_3$ due to the replacement of two Δ bonds per unit cell by six covalent bonds between

TABLE III. Cohesive energies of B_{12} , C, and $B_{12}C_3$ together with the heat of formation of $B_{12}C_3$.

$E_{\text{coh}}(B_{12})$	6.8402 eV/atom
$E_{\text{coh}}(C)$	8.3895 eV/atom
$E_{\text{coh}}(B_{12}C_3)$	7.2588 eV/atom
$H(B_{12}C_3)$	1.631 eV/unit cell

the icosahedra and the carbons in the CBC chain. We have also calculated the heat of formation $H(B_{12}C_3) = 15 E_{\text{coh}}(B_{12}C_3) - 3E_{\text{coh}}(C) - 12E_{\text{coh}}(B_{12}) = 1.631$ eV/unit cell, which is somewhat smaller than the experimental values¹¹⁻¹³ of 2.202, 1.795, and 1.94 eV/unit cell. Actually, it is the energy of the ground-state polymorph B_{105} which should be used to calculate $H(B_{12}C_3)$, which would make the discrepancy between our calculated value and experiment slightly larger. We also note that the total energy (valence electrons only) per unit cell² of $B_{12}C_3$ is 1391.8 eV, so that whatever the error in $H(B_{12}C_3)$, it is very small relative to the energies used to calculate it.

ACKNOWLEDGMENTS

This work was supported by the Robert A. Welch Foundation (Houston, Texas), the University of Texas Center for High Performance Computing, the Texas Advanced Research Program, and the National Science Foundation under Grant No. DMR-8718048.

¹J. L. Hoard and R. E. Hughes, in *The Chemistry of Boron and Its Compounds*, edited by E. L. Muetterties (Wiley, New York, 1967), p. 25.

²D. M. Bylander, L. Kleinman, and S. Lee, *Phys. Rev. B* **42**, 1400 (1990).

³C. Wood and D. Emin, *Phys. Rev. B* **29**, 4582 (1984).

⁴D. R. Tallant, T. L. Aselage, A. N. Campbell, and D. Emin, *Phys. Rev. B* **40**, 5649 (1989).

⁵H. J. Becher, *Z. Anorg. Allg. Chemie* **306**, 266 (1960); **321**, 217 (1963).

⁶We started this calculation with the same cutoff used for $B_{12}C_3$ but as we converged to the equilibrium lattice constant and angle we kept the number of plane waves fixed.

⁷B. F. Decker and J. S. Kasper, *Acta Crystallogr.* **12**, 503 (1959).

⁸F. H. Horn, *J. Appl. Phys.* **30**, 1611 (1959); in *Boron-Synthesis*,

Structure, and Properties, edited by J. A. Kohn, W. F. Nye, and G. K. Gaulé (Plenum, New York, 1960), p. 110.

⁹The symmetries at Γ are described in the caption of Fig. 2. For example, $\Gamma_1^{-(3)}$ means the third odd (under inversion) nondegenerate state at Γ which is even under reflection.

¹⁰C. Kittel, *Introduction to Solid State Physics*, 6th ed. (Wiley, New York, 1986), p. 55.

¹¹*CRC Handbook of Chemistry and Physics* (CRC, Boca Raton, 1989), Vol. 70, D55.

¹²D. Smith, A. S. Dworkin, and E. R. Van Artsdalen, *J. Am. Chem. Soc.* **77**, 2654 (1955).

¹³M. W. Chase, Jr., C. A. Davies, J. R. Downey, Jr., D. J. Frurip, R. A. McDonald, and A. N. Syverud, *J. Phys. Chem. Ref. Data* **1**, Suppl. 1, 451 (1985).